Intricate Multiscale Mechanical Behaviors of Natural Fish-Scale Composites

Chapter · April 2013
DOI: 10.13140/2.1.2868.0643

3 authors:

Deju Zhu
Hunan University
77 PUBLICATIONS **899** CITATIONS
SEE PROFILE

Francois Barthelat
McGill University
104 PUBLICATIONS **2,925** CITATIONS
SEE PROFILE

Franck J Vernerey
University of Colorado Boulder
80 PUBLICATIONS **1,272** CITATIONS
SEE PROFILE

Chapter 25

Intricate Multiscale Mechanical Behaviors of Natural Fish-Scale Composites

Deju Zhu,[a] Francois Barthelat,[a] and Franck Vernerey[b]

[a] *Department of Mechanical Engineering, McGill University, Montreal, QC H3A 2K6, Canada*
[b] *Department of Civil, Environmental and Architectural Engineering, University of Colorado, Boulder, CO, 80309, USA*
francois.barthelat@mcgill.ca, franck.vernerey@colorado.edu

25.1 Introduction

Millions of years of evolution and natural selection have yielded biological materials constructed for optimal structural performances [1]. Nature therefore increasingly serves as a model and inspiration to scientists and engineers. Biomimetics (the process of mimicking nature) has the potential to lead to novel engineering materials and systems with new combinations of properties, multi-functionalities, adaptability and environmental sustainability. Natural and man-made materials often share the same specifications and design constraints: structural support,

Handbook of Micromechanics and Nanomechanics
Edited by Shaofan Li and Xin-Lin Gao

ISBN 978-981-4411-23-3 (Hardcover), 978-981-4411-24-0 (eBook)
www.panstanford.com

lightweight or protection against certain threats. However, in most cases, nature takes a different route to solving engineering problems [2], and does so by adopting highly efficient solutions. Nature can therefore serve as a significant source of inspiration for new and alternative engineering designs. Following these principles, biomimetics has recently started to yield materials with remarkable properties [3]. The natural materials that served as "models" for these recent developments include seashells [4] , glass sponge skeleton [5] or toucan beaks [6]. Made of relatively weak materials, the mechanical performance of these natural materials comes from their microstructure, often complex and arranged over several distinct length scales (hierarchical structure). A fundamental understanding of the relationship between structure and function is therefore required and will give invaluable insight in how to design tomorrow's engineering materials [3].

The scaled skin of fishes is another example of a natural material with remarkable mechanical properties: compliance, resistance to penetration, light weight, and ultra-thin structure. Fish scales exhibit a great variability in shape, size and arrangement. The general classification includes cosmoid, ganoid, placoid, and elasmoid (cycloid and ctenoid) found in the modern teleost class of fishes [7]. The "primitive" cosmoid and ganoid scales are bulky, bony scales which offer very effective protective properties, through a multilayered structure capable of a variety of dissipative mechanisms [8]. Over the course of evolution the reduction of the integumental skeleton has improved swimming performance [9], and the "ancient" cosmoid and ganoid scales have been replaced by the thinner, more flexible teleost scales [10]. Teleost scales have excellent hydrodynamic properties [11] and provide a protective layer resisting penetration and in fact, teleost fish scales are so tough that they cannot be easily fractured even after immersion in liquid nitrogen [12]. At larger lengths, the arrangement of the scales provides a flexible skin that allows for changes in shape. In fact, the scaled skin has been shown to play a critical structural role in fish locomotion by regulating wave propagation and by storing mechanical energy in order to make swimming more efficient [13, 14]. Overall, the mechanics of fish-scales has received relatively little attention from the materials development community [15–17].

25.2 The Hierarchical Structure of Fish Scales

A paradigm in the construction of natural materials from basic "building blocks" such as amino acids or nano-flakes of mineral is hierarchy [18, 19]. Teleost fish scales display a characteristic hierarchical structure, as depicted on Fig. 25.1. At the macroscopic level, the scales are staggered and cover most of the body of the fish (Fig. 25.1a). This arrangement provides a continuous barrier to penetration, together with flexural compliance. When the fish is highly curved at the end of a swimming stroke, the scales interact more strongly, which stiffens the skin in flexion [20]. The skin then acts as an "external tendon", storing mechanical energy, which can be recovered to help initiate the next stroke [14]. At the mesoscale level, an individual scale from an adult striped bass is a thin plate with an irregular pentagonal shape, about 10 mm in diameter (Fig. 25.1b).

The posterior area of the scale displays rough patterns (ctenii) that offer attractive hydrodynamic properties [11, 21], while the anterior area consists of grooves in the radial direction (radii) and ridges that form circular rings (circuli) around a central area called the 'focus' [22] (Fig. 25.1b). Teleost scales are composed of collagen fibrils type-I, and are partially mineralized with hydroxyapatite [17]. In terms of composition, fish scales are therefore similar to bone. The outer layer of the scale is significantly more mineralized and often referred to as "bony layer", whereas the inner layer ("basal" or "collagen" layer) is mineralized mostly near the bony layer [9]. In striped bass, bony and collagen layers have approximately the same thickness (100 μm). An average hydroxyapatite mass fraction of 46% (26% in volume fraction) was determined by using AES (atomic emission spectroscopy) for the whole scale. The bony layer is much mineralized (50% hydroxyapatite mass content) compared to the collagen layer (14% hydroxyapatite mass content).

Bony and collagen layers are cross-ply layered composites, each ply being made of parallel collagen fibrils rotated across layers by different angles across species [23]. In striped bass, the basal layer consists of 20–25 plies about 4–5 μm thick each (Fig. 25.1c), where the collagen fibrils are rotated by 90 degrees from one ply to the next (Fig. 25.1d). At smaller length scales, individual collagen fibrils,

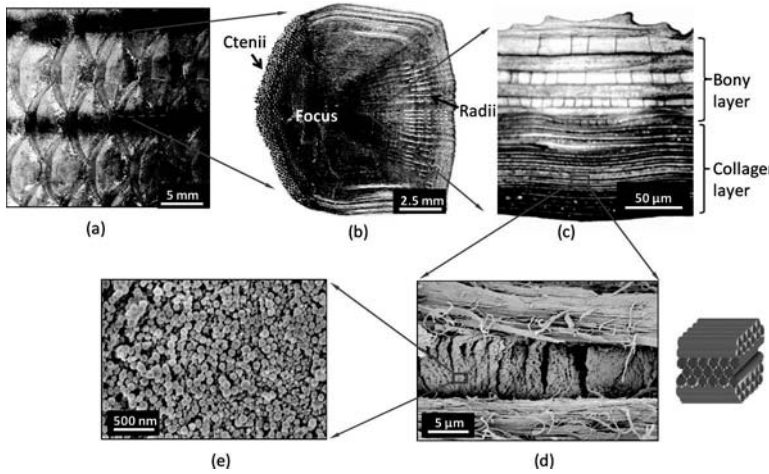

Figure 25.1 The hierarchical structure of a teleost fish scale from striped bass, *M. saxatilis*. See also Color Insert.

about 50 to 100 nm in diameter, can be observed on a cross section of the scale (Fig. 25.1e). In striped bass the 90 degree cross-ply is achieved by alternating layers composed of radial fibrils ("R" layers) with layers made of circumferential fibrils ("C" layers), both layers being organized around the focus of the scale (Fig. 25.2). This arrangement is consistent with the growth of individual scales, which occurs by deposition of collagen at the periphery of the scale [24].

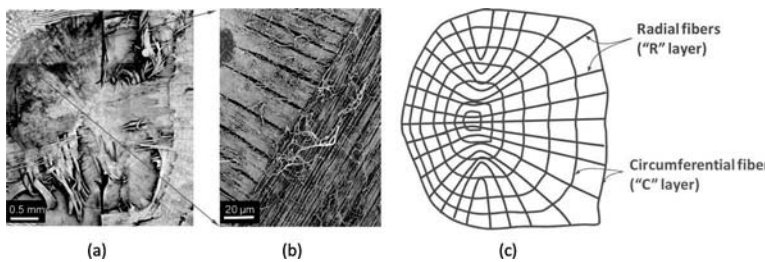

Figure 25.2 Arrangement of the collagen fibrils in a striped bass scale: (a) removal of the bony layer reveals the radial-circumferential (R-C) pattern of the collagen fibrils; (b) the fibers are orthogonal from one layer to the next; and (c) schematics of the R-C pattern. See also Color Insert.

25.3 Tensile Testing of Individual Scales

Small scale tensile tests can reveal the basic mechanical properties of individual scales and of the two layers that composes them. Here scales were plucked from fresh striped bass (*Morone saxatilis*) using tweezers and stored in a freezer at –20°C until tested. Before the test, the scales were removed from the freezer and put in a water bath for about 5 minutes for thawing, and then cut into small dog-bone-shaped specimens with a gage length of 4 mm, a gage width of 1.5 mm and an average thickness of about 0.20 mm. Samples were cut at 0°, 45° and 90° from the anteroposterior axis of the fish in order to investigate the mechanical response along different directions. The samples were tested on a miniature loading stage (Ernest F. Fullam Inc., Latham, NY), which was placed under an upright light microscope (BX-51M, Olympus, Markham, Canada) equipped with a CCD camera in order to monitor deformations and failure modes of the specimens. All specimens were loaded in tension at a rate of 0.005 mm/s (corresponding to a strain rate of 1.25×10^{-3} s^{-1}) up to complete failure. Images were taken throughout the entire test every 10 seconds using the CCD camera. The images were used to measure the deformation and strain values of the samples using digital image correlation [25] and to monitor failure modes such as debonding of the bony layer and pullout of the collagen fibrils.

The resulting stress–strain curves (Fig. 25.3) display an initial quasi-linear region with an initial modulus in the range of 600–850 MPa. The material softens slightly before reaching a maximum stress of 30–50 MPa, after which the stress drops significantly. The optical images show this sudden decrease in stress can be attributed to the sudden cracking of the bony layer. Subsequently, the collagen layer progressively detaches from the bony layer, while collagen plies tear one after the other, yielding step-like patterns on the stress–strain curves up to total failure at about 40% strain. In order to assess the mechanical response of the collagen layer alone, additional tensile tests were performed on scales with the bony layer removed. The collagen layer was carefully peeled out of the scale. The layered structure of the fish scale makes it easy to "delaminate" with a minimum of force. While the collagen material at the separation site might be partially damaged, the peeling force

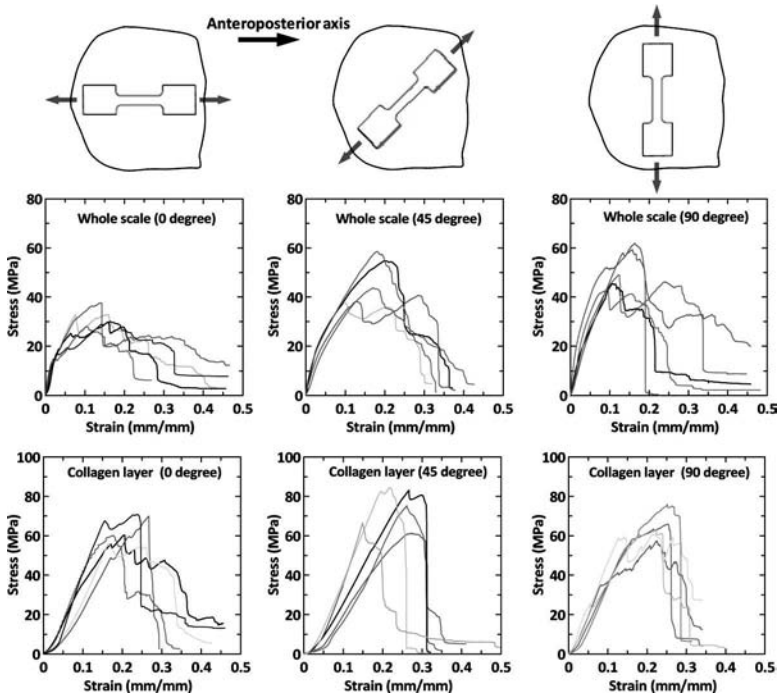

Figure 25.3 Tensile stress–strain curves for whole scales and collagen layer along 0°, 45° and 90° from the anteroposterior axis of the fish.

was deemed insufficient to damage the rest of the collagen layer and to alter its overall mechanical properties. The remaining 0.05 mm thick collagenous material was tested in tension along the 0°, 45° and 90° directions. The stress–strain responses of collagen layer (Fig. 25.3) display a linear regime with a modulus of about 450 MPa, followed by a progressive failure after a peak stress of 65 MPa. The ultimate strain was the same with and without the bony layer. The behavior of the collagen cross-ply is consistent with the behavior of single collagen type I fibrils [26]. Assuming that the fibers do not carry any stress if they are perpendicular to the loading direction, only half of the material actually carries stress in the collagen layer. Since individual collagen fibrils have Young's modulus of about 1 GPa, a tensile strength of 200 MPa and a strain at failure of 30% [26], the modulus of the 90° ply laminate can be estimated at 500 MPa, its

strength at 100 MPa and its strain at failure at 30%. This compares well with current experimental results, showing that the tensile behavior of the collagen layer is largely controlled by the stretching of straight, individual collagen fibrils.

While it was not possible to isolate the bony layer for testing, its properties were inferred from the whole scale and collagen only tensile test results. In the elastic regime, the whole scale behaves like a two-layer, constant strain composite. Since the thickness of the bony and collagen layers is similar, the modulus of the scale is given by

$$E_S = \frac{1}{2}(E_C + E_B) \tag{25.1}$$

where E_C and E_B are Young's moduli of collagen and bony layers, respectively. The modulus of bony layer can then be estimated by using

$$E_B = 2E_S - E_C \tag{25.2}$$

The strength of bony layer can be evaluated with a similar approach. In the linear regime, with the uniform strain assumption, the stresses in the bony and collagen layers are proportional to their stiffnesses. From the whole scale test, the stress σ_S at which the bony layer fails is known. Just prior to failure the stress in the bony layer is then given by

$$\sigma_B = \frac{E_B}{E_S}\sigma_S \tag{25.3}$$

This method assumes that both materials are in the linear elastic range up to the failure of the bony layer. Figure 25.3 shows that the scale softens slightly when loaded in tension; probably due to damage accumulation in the bony layer (collagen behaves linearly over this range of strain). Equation 3 therefore slightly overestimates the actual strength of the bony layer. The results show that the bony layer is about twice as stiff as the collagen layer, with about the same tensile strength (Fig. 25.4). The bony layer is however more brittle, failing at about 10% strain while the collagen layer fails at strains in excess of 40%. The whole scale displays in-plane anisotropic properties, but only because of the bony layer; the collagen layer is isotropic in plane in terms of both modulus and

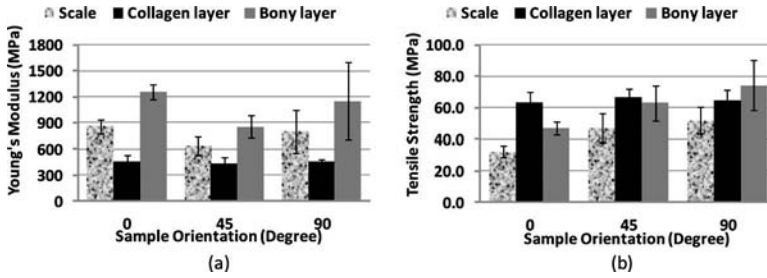

Figure 25.4 Summary of results for (a) Young's modulus and (b) tensile strength. The error bars indicate standard deviations.

strength. This set of experiments highlights the main characteristics of the fish scale's components: the bony layer is stiff, hard and brittle because of its high mineral content, while the underlying collagen cross-ply is softer and more deformable with larger strains at failure.

25.4 Resistance to Sharp Penetration

The main function of fish scales is to provide mechanical protection against predators [8] and, in particular, the scale must be capable of preventing sharp objects such as the teeth of predators [27] from completely penetrating the skin. The resistance to penetration of single striped bass scales was assessed by using an experimental setup that simulates a predator's bite. A sharp steel needle (tip radius $= 25$ μm) was driven through a scale resting on a silicone rubber substrate ($E \sim 1.8$ MPa) used to simulate the soft dermis and tissues underlying the scale (Fig. 25.5a). The resulting load–displacement curves were highly repeatable with a slight force drop at about 2.2 N and a maximum penetration force of 3 to 4 N (Fig. 25.5b). For comparison, puncture tests were performed on thin polystyrene (PS) and polycarbonate (PC), which are modern engineering polymers typically used in CD cases, biomedical equipments, and protective gears where light weight, stiffness, strength, optical translucence and impact resistance are required. For proper comparison 10 mm diameter disks of these polymers were prepared, and the thickness was adjusted so the areal density

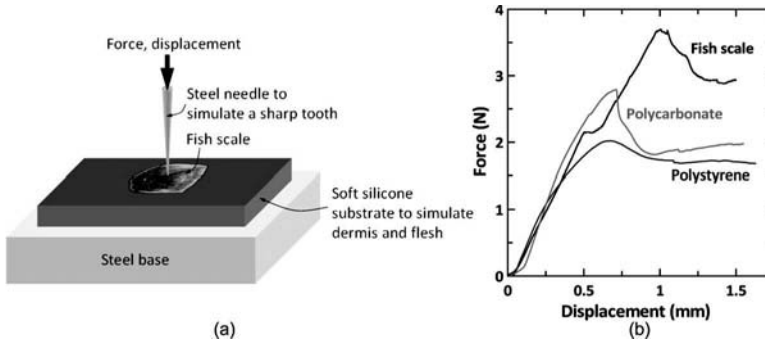

Figure 25.5 (a) Experimental setup of the puncture test; (b) typical force-displacement curves of striped bass scales, polystyrene and polycarbonate disks.

(the mass per unit area) of the protective layer was then same for fish scale, PC and PS. Remarkably, the fish scale provided a significantly higher resistance to puncture compared to these high performance engineering polymers (Fig. 25.5b).

The penetration curves consist of three distinct stages investigated in detail by imaging of the puncture site at different points on the penetration curve (Fig. 25.6). Stage I is the initial linear region, which is dominated by flexion of the entire scale and by damage and indentation of the surface of the bony layer. At a force of about 2.2 N, the force drops slightly, which is associated to the sudden cracking of the bony layer. Bony and collagen layers have the same thickness, but since the bony layer is stiffer, the neutral plane of the scale lies within the bony layer. As a result, flexural deformations generate tensile stresses in the lower side of the bony layer. Once these stresses reach the tensile strength of the bony layer [28], cracks initiate at the collagen/bone interface and rapidly propagate toward the surface of the bony layer. Interestingly, the patterns of the flexural cracks always followed a cross pattern, whose orientation invariably followed the orientation of the local radii and circuli (Fig. 25.6b) and underlying collagen fibrils. The microstructure of the bony layer therefore induces the failure of the bony layer along specific directions. Upon cracking of the bony layer, four "flaps" of bony material immediately deflect downwards, generating circumferential cracks. The underlying collagen layer,

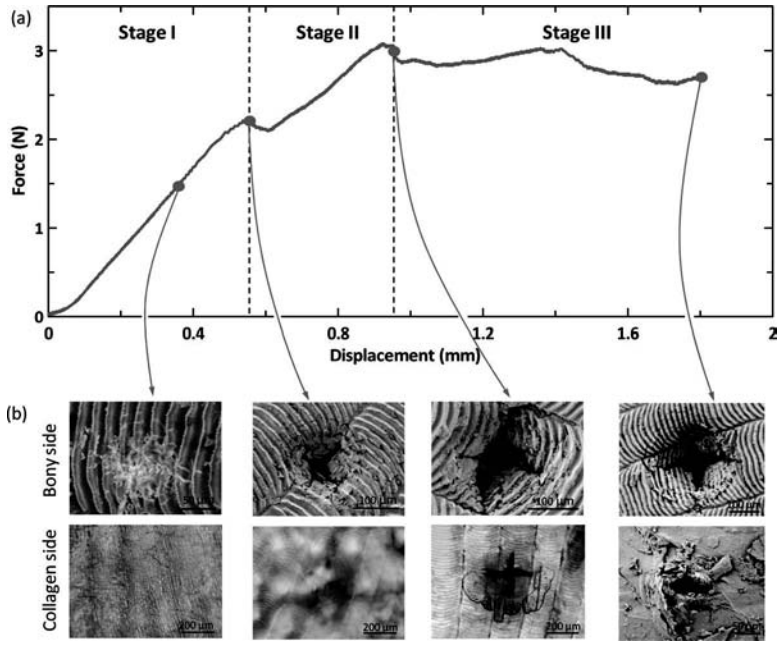

Figure 25.6 (a) Load–displacement curve showing three distinct stages; (b) images of the bony and collagen sides. See also Color Insert.

while remaining intact, detaches from the bony layer over a ring-like area observable with the optical microscope. The cracking of the bony layer marks the beginning of stage II, dominated by further flexion of the scale, radial propagation of the cross cracks as the four "flaps" of bony material are bent toward the collagen layer, and further delamination between collagen and bony layers. Eventually the deflection and opening of the flaps are sufficient to let the needle reach the collagen layer and completely puncture it (stage III). The initial failure of the collagen layer indicates the beginning of stage III, and the sharp drop in force at this point suggests that the failure is rapid, possibly because the collagen layer is stretched. Throughout the rest of stage III, the scale is deflected by the needle, the delamination between collagen and bony layers propagates more extensively, and the radial cracks continue to grow.

25.5 Analytical Model

The mechanisms operating at stage II were investigated, since they are powerful enough to increase the resistance of the scale by an additional 1 N. In particular, the controlled deflection of the four "bony flaps" was examined using an idealized three-dimensional geometry shown in Fig. 25.7a,b. Each of the four flaps was assumed to be rigid and hinged along a straight line at the bone/collagen interface. The force from the needle was assumed to be evenly distributed on the flap tips. Only two loads can resist the deflection of the flaps by balancing the force from the needle: (i) the bending moment transmitted through the remaining ligament of the bony layer, and (ii) the intact collagen layer, which acts as a "retaining membrane" for the flaps and whose cross-ply structure is ideal for catching the flaps. The bending moment transmitted at the ligament was evaluated by assuming perfect plasticity in the bony layer with $\sigma_Y = 60$ MPa (evaluated from tensile tests). In order to balance this moment, the force applied by the needle was estimated at 1.2 N [29], which is actually below the force at which the bony layer fractures. This value represents an upper bound estimate, since in reality the bony layer probably cracks before the full plastic state can be reached. This prediction shows that in stage II, there is no bending moment transmitted at the bony flaps, and that the flaps can be assumed to rotate about frictionless hinges. The images show circumferential cracks in the region of the hinges, confirming that little or no bending moment can be transmitted though the bony hinge.

The second mechanism examined was associated with the collagen, which acts as a retaining membrane for the flaps. In the model (see [29] for details), the collagen layer was assumed to have completely delaminated from the overlying surface of the bony layer, which is consistent with experimental observations toward the end of stage II. The collagen layer then acts as a retaining membrane with biaxial tensile stress. Based on the idealized geometry, the moment balance of a single bony flap about the hinge led to a simple expression for the penetration force as a function of bony and collagen layer thickness (t_B, t_C), length of the flaps (L), and stiffness (E_C) and strength (σ_C) of the collagen layer. Full penetration at

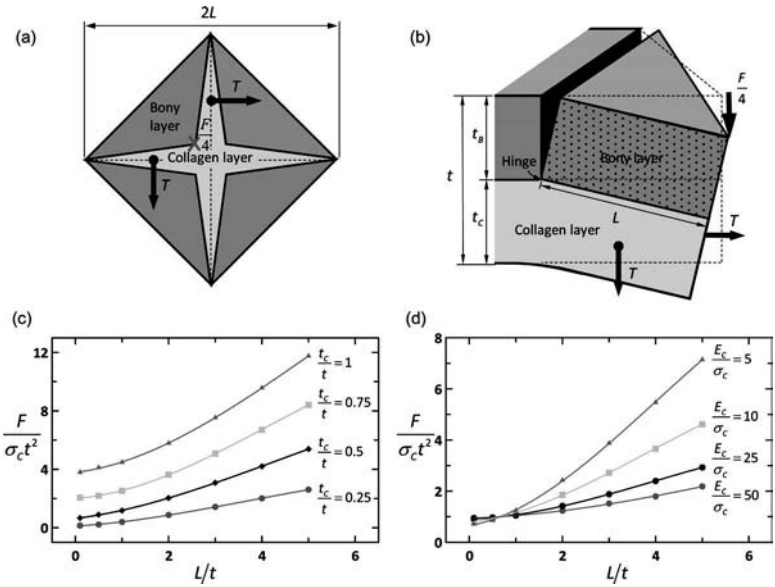

Figure 25.7 (a) Top view of the idealized puncture configuration; (b) three-dimensional view of single bony flap; (c) Effect of collagen layer thickness; and (d) collagen resilience on the normalized penetration force.

the end of stage II was assumed to be reached when the collagen failed in tension at a stress of 65 MPa according to the tensile tests. This model predicted a penetration force of $F = 3$ N based on the properties of the collagen layer ($E_C = 500$ MPa, $\sigma_C = 65$ MPa) and optical observation ($t_B = t_C = 100$ μm, $L = 200$ μm). This prediction is remarkably close to penetration force measured experimentally, which demonstrates that the retaining membrane effect dominates stage II and controls the ultimate penetration resistance of the scale.

In terms of design (Fig. 25.7c,d), the model reveals that longer flaps are desirable, indicating that the scale provides a greater resistance to penetration for larger teeth and stronger bites. A thick collagen layer is also beneficial, although a minimum of bony material is required to form stiff flaps. Finally, a soft and strong material increases resistance to penetration, although a too soft backing layer may lead to excessive deflection that may damage the

underlying tissues even before needle penetration. A cross-ply of collagen is therefore ideal for this function, and the harder bony layer is to protect the collagen layer from direct contact with the needle tip, and to mitigate the stresses transmitted onto the softer collagen layer by redistributing them over a large area.

25.6 Interaction between Scales

Overlapping of individual scales make a larger protective system covering the entire body of the fish. While resistance to penetration is critical for individual scales, flexibility is also an important attribute for the skin as a whole. The flexibility of the skin in bending is actually also controlled by the interaction between scales. The mechanics of fish skin and its interaction with the surrounding organs and, muscles and skeletal structure is very complex. This section concentrates on the deformation of a population of elastic scales on the surface of dermis of fish and understand how they affect the overall mechanical behavior of the skin. This study also seeks to quantify the changes in overall skin properties in bending due to modifications in scale shape, arrangement and properties [20].

25.6.1 *Analytical Model*

Following fundamental engineering and homogenization principles [30], this problem can be investigated by introducing an idealized model of fish scale structures, which, despite its simplicity, contains the principal ingredients of fish scale deformation during bending. The idealized model of fish scale structure can thus be described as follows. In its initial configuration, the scale structure is represented as a two-dimensional arrangement of initially straight scales, lying on a straight support. Scale deformation is then restricted by its attachment to the support (on its left end) and a rotational spring resisting scale rotation at its attachment point. Assuming that the support's rigidity is large in comparison to that of individual scales, its deformation is described in terms of homogeneous curvature κ. In other words, during bending, the support shape is described

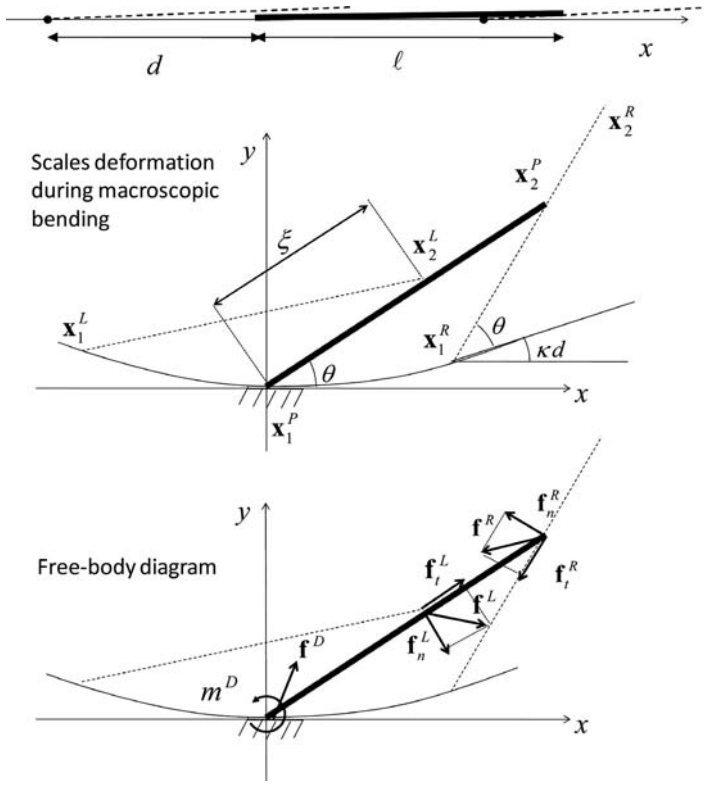

Figure 25.8 Initial, deformed configuration and free body diagram of a primary (representative) scale (bold line) during macroscopic bending. Adjacent (left and right) scales are also shown by dotted lines for clarity.

as an arc circle of radius $R = 1/\kappa$ (Fig. 25.8), which results in the rotation and deformation of scales and the development of contact forces between adjacent scales. The elastic energy stored in this deformed configuration determines the bending stiffness of the fish-structure. To further simplify the system, one may take advantage of two distinct features of fish scale structure: (i) the fish scale structure is made of a periodic pattern and (ii) during uniform bending deformation, every scale undergoes the same deformation. These hypotheses allow us to greatly reduce the size of the problem by considering the mechanics of a single representative fish scale instead of a large assembly of them. Microstructural

characteristics such as scale size, arrangement, and properties can thus be entirely described in terms of this single scale geometry and applied boundary conditions (Fig. 25.8). This simple model can then be used obtain a relationship between the macroscopic response of a scaled skin and the nature of its underlying structure. The free-body diagram of a fish scale subjected to several applied forces and moments arising from dermis–scale and scale–scale interactions is depicted in Fig. 25.8. In particular, the following are considered:

The force exerted by the left scale applied at the point of contact. This force is comprised of a normal force f_n^L and a tangential force f_t^L resulting from friction. The force exerted by the right scale applied at the right extremity of the principal scale. This force can also be decomposed into a normal f_n^R and tangential f_t^R component, with respect to the right scale. Because of the periodicity argument, the magnitude of these forces is equal and opposite to f_n^L and f_t^L. A moment m^D resisting scale rotation around its support.

In this model, assumption of a constant curvature of the support allows us to neglect the effect of local support deformation and concentrate on the response from fish scales exclusively. The above model implicitly assumes that the contact between scales can be considered a point-wise interaction. While this situation may differ slightly from a real distributed scale–scale contact, this assumption will provide a first good approximation of the interaction. The model will thus consist of computing the equilibrium configuration of the representative scale for different values of the overall (macroscale) curvature κ. Referring to Fig. 25.8, as κ is varied, the position of the right scale (and thus the force f^R) changes. This results in a redistribution of forces and moment in the scale and at the contact points. The elastic energy stored in the system can then be computed and used to determine the macroscopic elastic energy, which in turn is used to compute the macroscopic moment. This procedure therefore permits the determination of the macroscopic moment-curvature response.

Deformation of a single scale

In the two dimensional analysis, the cross section of a scale is viewed as a beam undergoing a combination of shear, axial and bending

deformations. During macroscale bending, each scale may undergo a significant amount of deformation depending to their geometry and properties. It is thus essential to incorporate the nonlinear effect of finite rotation and deformation into the model. The approach taken in this analysis relies on a hybrid analytical-computational formulation for which details can be found in [31]. In a nutshell, the method consists of solving a nonlinear ordinary differential equation for the orientation ϕ of the beam's centroid, that takes the following form:

$$U = E I \frac{\partial^2}{\partial s^2} (\phi - \phi_0) + g(s) = 0 \tag{25.4}$$

where E and I are the are Young's modulus and moment of inertia of the scale's cross section, respectively, ϕ_0 is the initial orientation of the beam's centroid and s is the curvilinear coordinate, referring to the initial scale configuration. The function g is a nonlinear function of the beam's orientation and the applied forces whose general expression is given by

$$g(s) = w \diamond F + \alpha F \cdot P_1 - m \tag{25.5}$$

where operation $\diamond$ is defined as $w \diamond F = w_x F_y - w_y F_x$ and the vector w and matrix $P_1 = \begin{bmatrix} -\sin 2\phi & \cos 2\phi \\ \cos 2\phi & \sin 2\phi \end{bmatrix}$ are functions of the beam's orientation. In addition, F is an integral measure of the forces f^L, f^R applied on the beam (see [20] for details) and m is the applied moment at point s. In this particular case,

$$m(0) = m^D \text{ and } m = 0 \text{ when } x \neq 0 \tag{25.6}$$

Finally, the constant α is written in term of the shear modulus G, axial modulus E and the beam cross section A as follows:

$$\alpha = \frac{1}{2} \left(\frac{1}{E A} - \frac{1}{G A} \right) \tag{25.7}$$

Upon solving for the beam's orientation $\phi = \phi(s)$, the deformed shape of the scale, given by the coordinate $x = (x(s), y(s))$ of points on the centroid, is calculated as follows:

$$x(s) = x(0) + \int_0^s q(\phi(\xi)) d\xi \tag{25.8}$$

where the expression for q is an explicit function of ϕ and applied forces that takes the form:

$$q(\phi) = w + P_2 \cdot F \tag{25.9}$$

where matrix $P_2 = \begin{bmatrix} \beta + \alpha\cos 2\phi & \alpha \sin 2\phi \\ \alpha \sin 2\phi & \beta + \alpha \cos 2\phi \end{bmatrix}$, $\beta = \frac{1}{2}\left(\frac{1}{EA} + \frac{1}{kGA}\right)$. The above formulation is a very efficient way to investigate the large deformation of a beam, including bending, shear, axial deformation and buckling.

Scale–scale and dermis–scale interaction

In addition to scale deformation, the model should characterize the magnitude, direction and point of application of scale–scale forces as well as the moment m^D representing the attachment between scale and dermis. For this, let us define f as the magnitude of the normal contact force between two scales, ξ as the coordinate of the contact point, measured from the attachment in the curvilinear coordinate system and κ as the macroscale curvature. Denoting n_ξ as the unit vector normal to the scale centroid at contact point ξ, the normal contact force f_n^L is written:

$$f_n^L = -fn_\xi \tag{25.10}$$

In order to compute the contact force f_n^R, the orientation difference between two adjacent scales is given by the product κd, where d is the inter-scale distance (Fig. 25.8). Thus, it is straightforward to show that

$$f_n^R = fR \cdot n_\xi \tag{25.11}$$

where $R = \begin{bmatrix} \cos\kappa d & -\sin\kappa d \\ \sin\kappa d & \cos\kappa d \end{bmatrix}$ is the orthogonal rotation matrix associated with a rotation of angle κd. The tangential forces at contact points are then related to their normal counterpart and the friction coefficient c as follows:

$$f_t^L = cQ \cdot f_n^L = -cfQ \cdot n_\xi \tag{25.12}$$

$$f_t^R = cQ \cdot f_n^R = cfQ \cdot R \cdot n_\xi \tag{25.13}$$

where Q = [0, −1 ; 1, 0] is the permutation matrix. Finally, the interaction between the dermis and the scale is given by a moment

m^D resisting the rotation of the scale at its attachment point, given by

$$m^D = K^D\left(\theta^S - \theta^D\right) = K^D\theta^S \tag{25.14}$$

where θ^D and θ^S are the rotation of the dermis and the scale at their point of intersection and K^D is the angular stiffness of the attachment. The rotation of the dermis θ^D vanishes for the representative scale.

25.6.2 *Results*

Figure 25.9 depicts the computed scale deformation for a macroscopic bending of $\kappa/l \approx 1$, with various values of scale bending and shear stiffness. Generally, if t is the thickness of the scale, the ratio GA/EI is comparable to $1/t^2$. In other words, a low relative shear resistance will be encountered for thick scales, while a high relative bending stiffness will be encountered when the scales become thin. The figure shows that different scale properties and geometry leads

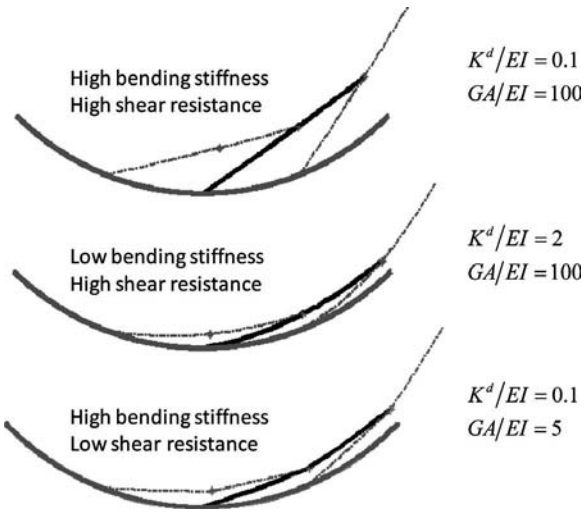

Figure 25.9 Scale centroid deformation for a macroscopic bending of $\kappa/l \approx 1$. Three situations are depicted depending on scale properties, relative to the rotational stiffness of the scale–dermis attachment. The "*" symbol refers to the contact point $x(\xi)$.

to very different deformation of the fish-scale structure. For clarity, the figure depicts the left and right scales, which undergo the same deformation as the primary scale. The results are shown for a scale discretization of 200 elements [20]. A high number of nodes were necessary in order to accurately capture the location of the contact force.

An important result of this study is the presence of a strain-stiffening mechanism in fish-scale structure. Strain-stiffening response is a characteristic shared by a large number of biological structure and materials as a way to prevent structural damage and failure [32]. Indeed, a strain-stiffening material will tend to redistribute deformation over a large region in order to minimize the stored elastic energy. This feature ensures that stresses are dispersed throughout the structure. It plays a large role in preventing a localized unstable behavior of fish-skin during swimming and when a fish is subject to predator attack. The swimming activity of fish involves significant bending forces generated by powerful muscles. While the convex side of bending (undergoing stretching) is usually stable, the concave side may undergo an instability in the form of wrinkling if no scales are present (Fig. 25.10a). Wrinkling can be thought of as a localized instability associated with a decreasing resistance to bending as curvature increases. This localization, together with the large moment involved may result in injury or death of the fish. The design of the scaled-skin provides an excellent

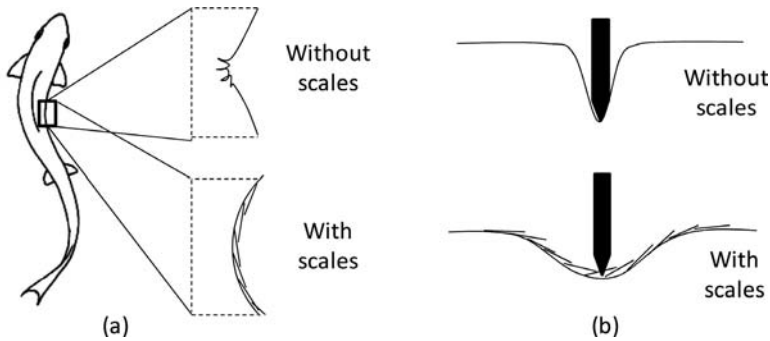

Figure 25.10 Illustration of the role of fish scales in preventing unstable localized deformation.

solution to prevent this kind of failure, due to its strain-stiffening behavior in the concave side of curvature. In addition, the role of fish scale as an external tendon is plausible, since the stored energy, which increases with curvature, may be restituted to the fish to increase locomotion speed. The scale structure could then be compared to a bouncing spring, converting its stored elastic energy into kinetic energy.

Another critical role of fish-scale structure is the protection of fish against a predator attack in the form of biting. From a mechanical view point, this situation can be compared to the indentation of a soft material (the fish body) covered with fish scales. As shown in Fig. 25.10b, the fish scale structure will (i) redistribute the curvature in a region whose size is proportional to scale size and (ii) due to the strain-stiffening response, an increasing indenting force will result in an increase of strain redistribution until failure of the indented scale occurs. Both features will contribute in minimizing force concentration, redistributing energy within the structure and thus retarding final failure.

25.7 Conclusions

Individual teleost fish scales are high performance natural protective systems, offering resistance to puncture superior to modern engineering polymers typically used for protective applications. Remarkably, fish scales are made of materials that are both softer and weaker than these engineering polymers, which highlights the important role of the structure of the scale in "amplifying" the properties, as seen in other biological materials [33–35]. The high performance of the scales attributes to a fine balance of structure and material properties, and in particular the hardness and stiffness of the outer layer, the softness and strength of the inner layer, and an interface weak enough to delaminate and allow the collagen layer to stretch under the bony flaps. The actual skin of the fish is covered with a large number of overlapping scales. For striped bass, any given point on the surface of the body is covered with three or four layers of scales. The resulting multilayer system alternates hard and soft layers in an arrangement reminiscent of the

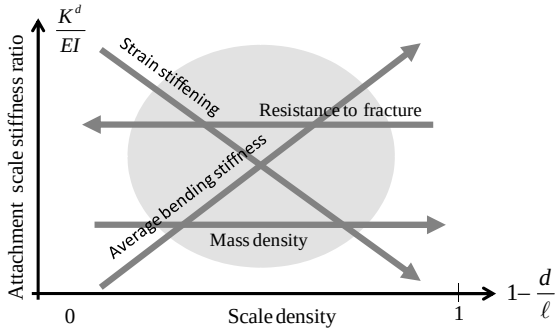

Figure 25.11 Trends of fish scale response in terms of its underlying microstructure.

design of bulletproof glass. In addition, overlapping scales ensures compliance and breathability, two highly desirable properties for personal armors. A biomimetic design at the individual scale level could therefore be combined with a clever arrangement of the scales at the macroscale to yield a hierarchical protective system with attractive properties.

The investigation on bending response of fish-scale structure in terms of its local geometry and properties shows that for certain microscale features, the response exhibits a strain-stiffening response, which can play a large role in preventing local unstable deformation during swimming and predator attack. Figure 25.11 summarizes the trends of fish scale response in terms of its underlying microstructure. According to its environment and size, a species of fish may emphasize certain functions over others. For instance, in cases where locomotion speed is emphasized, the structure will be "designed" in terms of the strain-stiffening (role of external tendon) and light weight. On the other hand, if protection against predator is critical, the design will favor a higher resistance to fracture and average bending stiffness. This flexibility in choice may explain the large diversity of scale structures encountered in nature, from large to small scale, high to low density, all of them within region of acceptable design depicted by the grey circle in Fig. 25.11.

References

1. Vogel, S., and K.K. Davis, *Cats' Paws and Catapults: Mechanical Worlds of Nature and People*. 2000: WW Norton & Company.
2. Sreidel Jr, R., and C. Makerov, *The Tensile Properties of Some Engineering Materials at Moderate Rates of Strain*. 1960, University of California, Livermore.
3. Barthelat, F., Biomimetics for next generation materials. *Philosophical Transactions of the Royal Society A—Mathematical Physical and Engineering Sciences*, 2007. **365**(1861): 2907–2919.
4. Wang, R.Z., *et al*., Deformation mechanisms in nacre. *Journal of Materials Research*, 2001. **16**(9): 2485–2493.
5. Aizenberg, J., *et al*., Skeleton of *Euplectella sp.*: Structural hierarchy from the nanoscale to the macroscale. *Science*, 2005. **309**(5732): 275–278.
6. Meyers, M., Toucan beaks engineered for strength and low density. *Advanced Materials & Processes*, 2006. **164**(1): 121–121.
7. Kardong, K.V., *Vertebrates: Comparative Anatomy, Function, Evolution*. 2008: McGraw-Hill New York.
8. Bruet, B.J.F., *et al*., Materials design principles of ancient fish armour. *Nature Materials*, 2008. **7**(9): 748–756.
9. Zylberberg, L., *et al*., Biomineralization in the integumental skeleton of the living lower vertebrates. *Bone*, 1992. **4**: 171–224.
10. Bereiter-Hahn, J., and L. Zylberberg, Regeneration of teleost fish scale. *Comparative Biochemistry and Physiology A—Physiology*, 1993. **105**(4): 625–641.
11. Sudo, S., *et al*., A study on the surface shape of fish scales. *JSME International Journal Series C—Mechanical Systems Machine Elements and Manufacturing*, 2002. **45**(4): 1100–1105.
12. Currey, J.D., The design of mineralised hard tissues for their mechanical functions. *Journal of Experimental Biology*, 1999. **202**(23): 3285–3294.
13. Long, J.H., *et al*., Biomimetic evolutionary analysis: testing the adaptive value of vertebrate tail stiffness in autonomous swimming robots. *Journal of Experimental Biology*, 2006. **209**(23): 4732–4746.
14. Hebrank, M.R., and J.H. Hebrank, The mechanics of fish Skin—lack of an external tendon role in 2 teleosts. *Biological Bulletin*, 1986. **171**(1): 236–247.
15. Wang, L.F., *et al*., Anisotropic design of a multilayered biological exoskeleton. *Journal of Materials Research*, 2009. **24**(12): 3477–3494.

16. Torres, F.G., *et al*., Characterization of the nanocomposite laminate structure occurring in fish scales from *Arapaima Gigas. Materials Science & Engineering C—Biomimetic and Supramolecular Systems*, 2008. **28**(8): 1276–1283.
17. Ikoma, T., *et al*., Microstructure, mechanical, and biomimetic properties of fish scales from Pagrus major. *Journal of Structural Biology*, 2003. **142**(3): 327–333.
18. Meyers, M.A., *et al*., Structural biological composites: An overview. *JOM Journal of the Minerals, Metals and Materials Society*, 2006. **58**(7): 35–41.
19. Fratzl, P., and R. Weinkamer, Nature's hierarchical materials. *Progress in Materials Science*, 2007. **52**(8): 1263–1334.
20. Vernerey, F.J., and F. Barthelat, On the mechanics of fishscale structures. *International Journal of Solids and Structures*, 2010. **47**(17): 2268–2275.
21. Sire, J.Y., Ontogenic development of surface ornamentation in the scales of *Hemichromis-Bimaculatus* (*Cichlidae*). *Journal of Fish Biology*, 1986. **28**(6): 713–724.
22. Jawad, L.A., Comparative morphology of scales of four teleost fishes from Sudan and Yemen. *Journal of Natural History*, 2005. **39**(28): 2643–2660.
23. Bigi, A., *et al*., Twisted plywood pattern of collagen fibrils in teleost scales: an X-ray diffraction investigation. *Journal of Structural Biology*, 2001. **136**(2): 137–143.
24. Ostrander, G.K., *The Laboratory Fish*, ed. G.R.B.T. Bunton. 2000, Oxford: Academic Press.
25. Barthelat, F., and J. Poissant, A novel "Subset Splitting" procedure for digital image correlation on discontinuous displacement fields. *Experimental Mechanics*, 2010. **50**(3): 353–364.
26. Shen, Z.L., *et al*., Stress–strain experiments on individual collagen fibrils. Biophysical Journal, 2008. **95**(8): 3956–3963.
27. Bemis, W.E., A. Giuliano, and B. McGuire, Structure, attachment, replacement and growth of teeth in bluefish*, Pomatomus saltatrix (Linnaeus, 1766)*, a teleost with deeply socketed teeth. *Zoology*, 2005. **108**(4): 317–327.
28. Seshaiya, R.V., P. Ambujabay, and M. Kalyani. Amino acid composition of Icthylepedin from fish scales. in *Aspects of Protein Structure Proceedings Symposium*, 1963. Madras.

29. Zhu, D., *et al*., Structure and mechanical performance of a "modern" fish scale. *Advanced Biomaterials*, 2011. In press (doi: 10.1002/adem.201180057).
30. Vernerey, F.J., *et al*., A micromorphic model for the multiple scale failure of heterogeneous materials. *Journal of the Mechanics and Physics of Solids*, 2008. **56**(4): 1320–1347.
31. Vernerey, F., and R. Pak, Analysis of soft fibers with kinematic constraints and cross-links by large deformation beam theory. *Journal of Engineering Mechanics*, 2011. **137**(8): 527–536.
32. Storm, C., *et al*., Nonlinear elasticity in biological gels. *Nature*, 2005. **435**(7039): 191–194.
33. Barthelat, F., and R. Rabiei, Toughness amplification in natural composites. *Journal of the Mechanics and Physics of Solids*, 2011. **59**(4): 829–840.
34. Buehler, M.J., Tu(r)ning weakness to strength. *Nano Today*, 2010. **5**(5): 379–383.
35. Keten, S., *et al*., Nanoconfinement controls stiffness, strength and mechanical toughness of beta-sheet crystals in silk. *Nature Materials*, 2010. **9**(4): 359–367.